Performance characteristics of UV imaging instrumentation for diffusion, dissolution and release testing studies

Jensen, Sabrine S; Jensen, Henrik; Goodall, David M; Østergaard, Jesper

Published in:
Journal of Pharmaceutical and Biomedical Analysis

DOI:
10.1016/j.jpba.2016.08.018

Publication date:
2016

Document version
Peer reviewed version

Performance characteristics of UV imaging instrumentation for diffusion, dissolution and release testing studies

Sabrine S. Jensen[a,b], Henrik Jensen[a], David M. Goodall[c] and Jesper Østergaard[a,*]

[a]Department of Pharmacy, Faculty of Health and Medical Sciences, University of Copenhagen, Universitetsparken 2, DK-2100 Copenhagen, Denmark.

[b]Present address: Novo Nordisk A/S, Novo Nordisk Park, DK-2760 Måløv, Denmark.

[c]Paraytec Limited, York House, Outgang Lane, Osbaldwick, York, YO19 5UP, United Kingdom

*Correspondence: Jesper Østergaard. Department of Pharmacy, Faculty of Health and Medical Sciences, University of Copenhagen, Universitetsparken 2, DK-2100 Copenhagen, Denmark. E-mail: jesper.ostergaard@sund.ku.dk, Telephone: +45 3533 6138, Fax: +45 3533 6001

This is a post-peer-review, pre-copyedit version of an article published in Journal of Pharmaceutical and Biomedical Analysis.

The final authenticated version is available online at: http://dx.doi.org/10.1016/j.jpba.2016.08.018

Abstract

UV imaging is capable of providing spatially and temporally resolved absorbance measurements, which is highly beneficial in drug diffusion, dissolution and release testing studies. For optimal planning and design of experiments, knowledge about the capabilities and limitations of the imaging system is required. The aim of this study was to characterize the performance of two commercially available UV imaging systems, the D100 and SDI. Lidocaine crystals, lidocaine containing solutions, and gels were applied in the practical assessment of the UV imaging systems. Dissolution of lidocaine from single crystals into phosphate buffer and 0.5% (w/v) agarose hydrogel at pH 7.4 was investigated to shed light on the importance of density gradients under dissolution conditions in the absence of convective flow. In addition, the resolution of the UV imaging systems was assessed by the use of grids. Resolution was found to be better in the vertical direction than the horizontal direction, consistent with the illumination geometry. The collimating lens in the SDI imaging system was shown to provide more uniform light intensity across the UV imaging area and resulted in better resolution as compared to the D100 imaging system (a system without a lens). Under optimal conditions, the resolution was determined to be 12.5 and 16.7 line pairs per mm (lp/mm) corresponding to line widths of 40 µm and 30 µm in the horizontal and vertical direction, respectively. Overall, the performance of the UV imaging systems was shown mainly to depend on collimation of light, the light path, the positioning of the object relative to the line of 100 micron fibres which forms the light source, and the distance of the object from the sensor surface.

Keywords: Dissolution imaging; Dissolution testing; Instrument performance; Spatial resolution; UV imaging

Abbreviations: API, active pharmaceutical ingredient; CARS, coherent anti-Stokes Raman Scattering Microscopy; CMOS, Complementary metal oxide semiconductor; FTIR, Fourier transform infrared; LOD, Limit of detection; MRI, magnetic resonance imaging; TDA, Taylor dispersion analysis.

1. Introduction

Dissolution and release testing is conducted for various purposes in the pharmaceutical industry e.g., to guide the drug development process, in quality control, and as biowaivers [1]. In the early phases of drug development, miniaturized or micro-scale techniques requiring low-milligram quantities of the active pharmaceutical ingredient (API) or formulation are of particular value [2-4]. Many dissolution and release testing methods are invasive methods and involve bulk solution concentration measurements by the withdrawal of test samples, which may disturb the subsequent release. In addition, the withdrawal of samples may also lead to delayed responses, due to the need for accumulation of the API in solution. Especially, in case of fast dissolution and release kinetics real-time analysis is advantageous. Better understanding of the dissolution or release behavior of an API or formulation may be attained using imaging techniques providing spatially, spectrally, and/or temporally resolved information. Imaging techniques used in pharmaceutical sciences for investigating drug dissolution and release processes include magnetic resonance imaging (MRI) [5-8], Fourier transform infrared (FTIR) imaging [4, 9-11], coherent anti-Stokes Raman Scattering Microscopy (CARS) imaging [12], fluorescence imaging

[13,14], and UV imaging [15,16]. UV imaging is compatible with a small scale format and has attracted attention as it offers insights into dissolution and release processes of drugs [17-27]. However, limited data are available regarding system performance of the commercially available UV imaging instrumentation. The current study was prompted by observations made during UV imaging experiments in our lab, and an associated wish to understand better the performance characteristics of the instrumentation, since this knowledge would be useful in the design, planning, and execution of future experiments. The purpose of the present study was to characterize two embodiments of a commercially-available UV imaging system in terms of analytical performance, including spatial resolution, linearity and noise. The instruments subject to study were an SDI (Sirius-Analytical, Forest Row, UK) and a D100 (Paraytec Ltd, York, UK) imaging system.

2. Experimental

2.1 Materials and sample preparations

Agarose (type I) was obtained from Sigma-Aldrich (St. Louis, MO, USA). Sodium hydroxide and sodium dihydrogenphosphate monohydrate were obtained from Merck (Darmstadt, Germany). Lidocaine (Ph Eur (European Pharmacopoeia) 6th ed.) was obtained from Unikem (Copenhagen, Denmark). Lidocaine crystals were prepared as described previously [16].

A 0.067 M phosphate buffered solution with an ionic strength of 0.15 M was prepared as follows. A weighed amount of sodium dihydrogenphosphate monohydrate (9.25 g) was transferred to a 1000 ml volumetric flask to which was then added de-ionized water to the neck

of the volumetric flask. The mixture was stirred at room temperature until the substance was dissolved, then the pH adjusted to 7.40 by adding 5 M NaOH.

For preparing the agarose hydrogels, a weighed amount of agarose powder, corresponding to 0.5% (w/v), was suspended in phosphate buffer at pH 7.4 followed by heating of the agarose suspensions to 98˚C for approximately 20 min to dissolve the agarose. The agarose solution (approximately 310 µl) was transferred to a quartz cell (8.0 mm × 1.0 mm × 38 mm (H × W × L)) (Starna Scientific Ltd, Hainault Essex, UK), and the lid of the cell placed on top of the agarose solution. Each quartz cell containing the agarose solution (the pre-gel) was left at room temperature for at least 0.5 h to ensure complete gelation of the agarose matrix.

The grids used for estimation of the resolution consisted of a black image made of silver halides (5 µm print layer thickness) coated on one side of a plastic base of polyester (180 µm thickness). The grids were produced under conditions of 21 °C at 50% humidity (JD Photo-Tools, Oldham, UK). The grids were drawn in AutoCAD software (Autodesk Inc., San Rafael, CA, USA). The width of the lines and the distance between the lines were identical and varied in the range 10 - 100 µm in 10 µm increments and then in 20 µm increments in the 100 to 400 µm range.

2.2 Instrumentation

The two imaging systems investigated, both utilizing ActiPix technology, were a D100 (Paraytec Ltd., York, UK) and an SDI (Sirius-Analytical, Forest Row UK). In terms of optical design [28,29], the Sirius SDI has improvements relative to the D100 through incorporating a lens for collimating the light in the direction parallel to the line of 90 x 100 µm optical fibres which

provide the 9 mm x 100 μm illumination source. The UV imaging systems are shown in Supplementary data Fig. S.1. The active pixel CMOS sensors have a total detection area of 9 mm × 7 mm consisting of 1280 × 1024 pixels with a size of 7 μm × 7 μm. Band pass filters with a band width of 10 nm were sourced from various manufacturers. Images were recorded and analyzed using ActiPix D100 software version 1.4 (Paraytec Ltd.). Images were recorded with a rate of 0.2 images per second, and the integration time was 10 ms. Pixel intensities were converted into absorbance using the ActiPix D100 software.

2.3 Methods and measurements

2.3.1 Linearity

Calibration curves of lidocaine in phosphate buffered solution at pH 7.4 in a concentration range of 5×10^{-6} - 1×10^{-2} M were constructed. Absorbance values of lidocaine solutions were measured in quartz cells with light paths of 1 and 4 mm at a wavelength of 214 or 254 nm using the SDI UV imaging system. The results were compared to results obtained using a conventional spectrophotometer (Shimadzu UV-1700, Shimadzu, Kyoto, Japan) and quartz cuvettes with a 10 mm light path.

2.3.2 Noise

Assessment of noise was made from the data recorded while preparing the lidocaine calibration curves in phosphate buffered solution at pH 7.4 using the Sirius SDI imaging system. Lidocaine

126 solutions were flowed through the flow cell with an ActiPix flow-through type dissolution
127 cartridge CADISS-3 (Paraytec Ltd.) at a flow rate of 1.0 ml/min. The pixels were binned 10 × 1
128 (x × y), the images were obtained at a rate of 1.15 frames per second, and the absorbance was
129 read from 5 effective pixel units positioned at different positions in the imaging area.

130

131 2.3.3 Resolution measurement using grids

132 Resolution measurements were carried out by placing the grid in an empty 1 mm quartz cell (8.0
133 mm × 1.0 mm × 36.0 mm (H × W × L)) or a 1 mm quartz cell filled with 0.067 M phosphate
134 buffered solution, pH 7.40, or 0.5% (w/v) agarose gel, pH 7.40. In these experiments, the grid is
135 located 1.2 mm above the cover slip of the sensor surface. Additional measurements were carried
136 out where the grid was placed directly on the cover slip of the sensor surface. Measurements
137 were performed at 610 nm with the pixels binned 1 × 1 and 4 × 4 using the D100 and the SDI
138 imaging systems. The resolution measured by the grids is given as the maximum number of line
139 pairs per mm (lp/mm) [30] for which the correct number of line pairs can be resolved by eye.

140

141 2.3.4 Resolution measured using lidocaine crystals

142 Lidocaine crystals were arranged in a quartz cuvette and imaged at 254 and 610 nm with pixel
143 binning of 1 × 1 or 4 × 4 using the SDI imaging system. The dimensions of the crystals were
144 furthermore measured using a Dino-Lite Premier Digital microscope (AM-7013MZT, AnMo
145 Electronics Corporation, Hsinchu, Taiwan) with a magnification of ×50.

146

147 2.3.5 Density gradients

148 Dissolution of lidocaine from single crystals was investigated in 0.067 M phosphate buffer, pH
149 7.4, and 0.5% w/v agarose gel, pH 7.4, in 1 mm quartz cells (see section 2.3.3) at 254 nm using
150 the SDI imaging system with pixels binned 4 × 4. To secure lidocaine single crystals during their
151 dissolution into 0.067 M phosphate buffered solution, pH 7.4, they were fixed at one end with
152 Bantex Tack-all removable adhesive (Bantex A/S, Lynge, Denmark) in the quartz cell.

153

154 2.3.6 Lidocaine diffusion in hydrogel

155 Diffusion of lidocaine from a 0.5% agarose gel at pH 7.4 loaded with 1 mM lidocaine into a
156 blank 0.5% agarose gel, pH 7.4, was studied using the SDI and D100 UV imaging systems in 1
157 mm quartz cells (see section 2.1). The D100 system was applied initially using the standard
158 setting and subsequently with the illumination source, the line end of the round-to-line fibre optic
159 cable, rotated by 90 ° (cf. section 2.2 for details on the line configuration of the fibre optic
160 bundle). The imaging was performed at a wavelength of 254 nm.

161 The diffusion coefficient (*D*) of lidocaine in the hydrogel matrix was determined from the UV
162 absorbance maps as a function of time by applying the following derivation of Fick's second law
163 [21,31]:

164 $$\frac{C(x,t)}{C_0} = \frac{1}{2} - \frac{1}{2} erf\left(\frac{x-x_0}{2\sqrt{t \cdot D}}\right) \quad (1)$$

where $C_{(x,t)}$ is the measured concentration as a function of distance and time, C_0 is the initial analyte concentration in the donor gel, *erf* is the error function, x_0 is the position of the interface between the gel phases and x is the distance from the gel-gel interface and t is the time. Eq. 1 is applicable for one-dimensional diffusion. In Eq. 1, the measured absorbance was used instead of the concentration, because the measured absorbance values were within the linear range according to Lambert Beer's law.

2.3.7 Diffusion coefficient of lidocaine in phosphate buffered solution

The diffusion coefficient of lidocaine in phosphate buffer at pH 7.4 was determined by Taylor dispersion analysis (TDA) at 25 °C as previously described by Ye et al. [32]. A sample of 5.0×10^{-3} M lidocaine in 0.067 M phosphate buffered solution was introduced into a fused silica capillary (75 µm (id) × 200 µm (od)) by pressure (50 mbar) for 7 s. The sample was forced through the capillary at a constant rate, and the broadening of the lidocaine sample plug due to convective diffusion was detected through two windows in the capillary by UV area imaging at 214 nm. The diffusion coefficient of lidocaine was determined from the peak appearance times and the variances of the Gaussian shaped peaks as described by Ye et al. [32].

3. Results and discussion

3.1 Performance characteristics of the UV imaging systems

The D100 UV imaging system was initially designed for use as detector in separation science [29,33-36]. Subsequently, applications in drug dissolution and release testing have emerged [20]. Fig. 1 shows a schematic representation of the basic UV imaging setup for monitoring surface dissolution. The prototype systems have been described in some detail [29,34-36], and methodology for capillary imaging with the D100 is covered elsewhere [28]. The key components include a pulsed Xe lamp emitting light in the wavelength range 190 to 1100 nm, 12.5 mm diameter band-pass filters with 10 nm bandwidth (22 nm at 214 nm) for wavelength selection, and a round-to-line fiber optical bundle, where the fibers are arranged in a line configuration at the end, presenting the light to the measurement zone (an array of 90 fibers with a diameter of 100 µm). The light is transmitted through the sample and reaches the detector part consisting of a cover slip, a layer of UV down-converting phosphor and an IBIS4 complementary metal oxide semiconductor (CMOS) sensor (Cypress, Mechelen, Belgium) with 1280 × 1024 pixels with dimensions of 7 µm × 7 µm (total imaging area 9 × 7 mm^2). The CMOS sensor is light sensitive in the range 400 to 1000 nm, thus the role of a UV down-converting phosphor layer (Gd_2O_2S:Tb) is to convert light in the UV wavelength range (190 - 290 nm) to the visible wavelength range (a line emission spectrum emitting at several wavelengths with the most prominent emission at 540 nm [37]), where the sensor is sensitive. The principles of UV converting phosphors are described elsewhere [38,39]. The associated electronics and software allow for the construction of images, which may be read in intensity or absorbance mode.

The UV imaging systems allow real-time monitoring of the experiments subject to study. Light intensity maps are displayed on a PC using the ActiPix software, and illustrated in Fig. 2 for the D100 and the Sirius SDI. With the D100 (Fig. 2A), the intensity distribution in the xy plane showing a maximum at y ~ 3 mm for all x is consistent with the line of fibres positioned above

the imager at y ~ 3 mm and aligned in the x direction. In the SDI system (Fig. 2B), the light intensity is more uniform across the imaging area, particularly in y direction; however, the light intensity is comparatively lower. The relatively uniform light intensity across the imaging area is related to the incorporation of a collimating lens in the SDI system, leading to a change in how the light is presented to the sample and sensor surface (cf. Fig. 3). The collimating lens constitutes the major difference between the two systems. The presentation of the light to the sample cell and sensor surface is of importance. This is further corroborated by measuring the apparent height from the lower to the upper surface of the flow cell (Fig. 1) to quantify the shadowing effect (Fig. 3). The directly measured height for the open section of this machined part was 3.44 mm. Apparent height values of 4.12 mm and 3.46 mm were reported from the ActiPix software from the images of the cell insert taken with the D100 and the Sirius SDI, respectively. The latter value is in good agreement with the true height, consistent with the light being fairly well collimated. The former value accords with a shadowing effect, in which light at any angle which hits the lower or upper surfaces of the insert is obscured.

When using the D100, this may contribute to the difficulties in calculating dissolution rates from UV images and matching those to dissolution rates obtained from the collected effluent, as was the case for paracetamol dissolution studies [20,40]. Also, so called surface concentrations obtained using a D100 UV imaging system should be considered as concentration estimates, since the line of fibres is centred at a y distance greater than the location of the lower surface of the cell insert, the first unobscured ray to reach the imager is transmitted through a layer of fluid significantly elevated from the surface.

3.1.1 Linearity, noise and LOD

UV imaging relies on the molecular absorbance of light. Pixel intensities are converted into absorbance using the instrument software according to:

$$A = \log\left(\frac{I_{ref} - I_d}{I_{sig} - I_d}\right) \quad (2)$$

where I_d, I_{ref} and I_{sig} are the ADC counts (a measure of intensity which will be referred to as pixel intensity in the following) due to the dark current (electronic noise measured with the lamp turned off), pixel intensity measured with the phosphate buffer (solvent) in the cell (reference signal), and pixel intensity measured during the experiment, respectively. The conversion into absorbance eliminates (to a large extent) the effects of non-uniformity of light intensity across the imaging surface as previously shown [41]. However, imaging artifacts have been observed, mainly in the edges of the images, which are related to low light intensity in this part of the imaging area (this has primarily been observed when using the D100 system). Examples of UV images showing such artifacts can be found in [42,43]. These imaging artifacts are most likely due to drift in the output of the light source over time, which will have the most predominant effect, when the light intensity is low. Drift in light intensity will mainly be an issue in release and diffusion studies, such as described in [42,43], where the self-referencing options of the software used in flow-through type dissolution studies cannot be applied.

The absorbance measured by UV imaging may be converted into concentration using Lambert Beer's law by the aid of a calibration curve. Deviations from Lambert Beer's law may occur due to a number of effects: the use of polychromatic rather than monochromatic radiation; the

presence of stray light; refractive index changes; close proximity of the absorbing molecules affecting their charge distribution and thereby altering their absorptivity; the molecules taking part in reactions (such as self-association and chemical degradation) and scattering effects due to particles [44-46]. The linearity of the system should therefore be investigated prior to dissolution and release testing experiments. Calibration curves obtained using the SDI imaging system for lidocaine solutions in quartz cells with light paths of 1 and 4 mm, and in a conventional spectrophotometer with a light path of 10 mm are shown in Fig. 4. The use of different instrumentation for absorbance measurements leads to the following apparent molar absorption coefficients (ε_{254}) at 254 nm: 6.2×10^2 M^{-1} cm^{-1}, 6.5×10^2 M^{-1} cm^{-1}, and 4.0×10^2 M^{-1} cm^{-1} (RSD < 4%; n = 3), when the light paths were 1 mm (SDI), 4 mm (SDI), and 10 mm (double beam spectrophotometer), respectively. At 214 nm the following apparent molar absorption coefficients (ε_{214}) were obtained: 4.7×10^3 M^{-1} cm^{-1}, 4.1×10^3 M^{-1} cm^{-1} and 11.2×10^3 M^{-1} cm^{-1} (RSD $\leq$ 7%; n = 3), when the light paths were 1, 4, and 10 mm, respectively. The calibration curves were constructed by averaging the absorbance values over a large part of the imaging area from absorbance readings over at least 1 min, in order to minimize the uncertainty and get the best estimate of the molar absorption coefficients. Fig. 4 shows that the calibration curves obtained by UV imaging bend off at absorbance values around 0.5 and 1 at light paths of 1 and 4 mm, respectively, while the calibration curve was linear up to an absorbance of approximately 2 at a light path of 10 mm using the conventional spectrophotometer. We have previously reported a ε_{254} of 4.36×10^2 M^{-1} cm^{-1} for lidocaine in the same phosphate buffer using a 3 mm light path quartz cell and an SDI300 imaging system (using a D100 sensor head configuration) [16]. The results show the importance of using a calibration curve that is constructed in the quartz cell, and using the band pass filter as well as the same system as the actual measurements will be

performed on. The performance of the total system is dependent on the light path, collimation of light and band pass width as well as the performance of the detector.

During the absorbance measurements of the standard solutions for construction of the calibration curves, the noise of the SDI imaging system was assessed. The peak to peak noise was estimated to be ~18 and ~35 mAU at 214 and 254 nm, respectively (Supplementary data Fig. S2; quartz cell with 4 mm light path). A higher light intensity at 214 nm is the reason for the lower noise level at 214 nm as compared to 254 nm. From the data shown in Supplementary data Fig. S2 and the slope of the calibration curve, the LOD (S/N = 3) for lidocaine in phosphate buffer was calculated to 3.3×10^{-5} M and 4.0×10^{-4} M at 214 and 254 nm, respectively. These LOD values are based on readings with individual effective pixels (10 × 1 binning), which together with the low molar absorption coefficients provide the reason for the relatively high LODs.

Fig. 5 shows detector response (pixel intensity) as a function of wavelength for the band-pass filters available in our lab using the SDI imaging instrument. The pixel intensities were read from the same area (5.60×4.76 mm^2) in all experiments to limit effects of the non-uniform intensity across the image surface. The detector response depends on the lamp intensity, transmittance of the band-pass filters, and efficiency of the UV down-converting phosphor in the UV range, and how these parameters vary as a function of the wavelength. Fig. 5 reveals a low pixel intensity/detector response in the wavelength interval 300 - 350 nm making UV imaging difficult in this range. The relatively poor performance in the range 300 - 350 nm results from the combination of a relatively low light output from the Xe lamp and poor efficiency of the UV down-converting phosphor (Gd_2O_2S:Tb [37]). These issues have also been described for a CCD detector utilizing UV down-converting phosphors [38,39]. Fig. 5 highlights another interesting

feature requiring attention in, namely that the transmission efficiency of the individual band pass filters vary.

3.1.2 Resolution of the UV imaging systems

Previous studies in our lab have indicated that the resolution of the UV imaging system is different in the horizontal (x) and vertical (y) direction. In the following, studies were performed to shed light on the resolution of the UV imaging systems. The resolution was assessed using grids with line pairs (a black and transparent line constitute a line pair) having widths between 10 and 400 µm. The line pair-width intervals were 10 µm below 100 µm, and 20 µm above 100 µm. The measurements were performed in the visible wavelength range, where the film is transparent and the grid lines absorb the light. Fig. 6 shows the absorbance maps of a grid with a line width of 100 µm placed on the cover slip of the sensor surface or in a quartz cell, leading to a position of the grid 1.2 mm above the cover slip of the sensor surface for the D100 and SDI imaging system due to the thickness of the quartz wall. High and low absorbance values are indicated by red and blue coloring, respectively, in the absorbance maps. A clear difference in the performance of the imaging systems in the x- and y-direction is seen from these images. This is due to the light coming from the fiber optic bundle with a line configuration above the CMOS chip (Fig. 3). An improved resolution is observed when the grid-lines are placed parallel to the light source line. In Table 1, the estimated resolution of the imaging systems is given as maximum line pairs per mm (lp/mm). In empty quartz cells and quartz cells filled with phosphate buffered solution or 0.5% (w/v) agarose hydrogel at pH 7.4, the resolution of the D100 and SDI imaging systems with pixels binned 4 × 4 (nominal resolution of 28 µm) were determined to be

316 1.7 and 2.5 lp/mm, respectively, in the x-direction and 10 and 12.5 lp/mm, respectively, in the y-
317 direction. A resolution of 12.5 lp/mm indicates that the system is able to separate and measure
318 lines with a width of 40 µm. According to Table 1, the resolution is substantially better when the
319 grid is placed directly on the cover slip of the sensor surface as compared to on the quartz cell.
320 Thus, the resolution depends on the position of the object above the cover slip of the sensor
321 surface, and it decreases as the object gets closer to the light emission slit. This can be seen as a
322 result of a shadowing / optical lever effect (Fig. 3 and section 3.1). The pixel-binning (1 × 1
323 versus 4 × 4) does not seem to have a large effect on the resolution. The results show that the
324 minimum resolvable feature size is greater than the size of the effective pixel. This is primarily
325 due to the optical lever effect combining the width of the light source (100 µm diameter for the
326 optical fibres) and the relatively short (9 mm) distance from fibre output to sensor surface. By
327 comparison with the D100, Table 1 highlights an improved resolution for the SDI due to
328 movement of the source to a greater distance away from the sensor surface and incorporation of a
329 collimating lens. The highest resolution was observed using the SDI system without any pixel
330 binning, when the grid was placed on the cover slip of the sensor surface, and was measured to
331 be 12.5 and 16.7 lp/mm (corresponding to line widths of 40 and 30 µm) in the x- and y-direction,
332 respectively.

333 Since the grids were not transparent in the UV range, and because the resolution also depends on
334 the level of contrast available, an alternative approach was developed to estimate resolution in
335 this spectral region which is of primary interest for dissolution studies. The dissolution of
336 lidocaine from selected single crystals into stagnant phosphate buffered solution has earlier been
337 investigated by UV imaging at 254 nm [16]. In order to show how the spatial resolution of the
338 two imaging systems influences the size and shape of the imaged objects, such lidocaine crystals

were imaged at wavelengths of 254 and 610 nm in the absence of dissolution medium. Microscope photographs and UV images of selected lidocaine crystals are shown in Fig. 7A and B. Both Fig. 6 and 7 show that the resolution of the imaging systems is better in the y-direction as compared to in the x-direction. In the current project, the width of the lidocaine crystal was measured at a selected position under the microscope to be 185.6 µm (Fig. 7A). The UV-Vis systems were able to identify and detect lidocaine crystals, but the width of the crystal placed parallel or perpendicular to the emission slit was measured to 230 or 480 µm, respectively, by the SDI system with pixels binned 4 x 4 at 254 nm (Figs. 7B and C). It is evident that UV-Vis imaging overestimates the thickness of the lidocaine crystal; this is due to the optical lever and shadowing effects with the object (Fig. 7B).

Absorbance - distance profiles were constructed from the absorbance maps of the lidocaine crystals, and the resolution of the imaging system was determined based on the sharpness of the interface, as previously described by Chan et al. [47], by measuring the distance over which the normalized absorbance fell from 95 to 5 % of the maximum value. The normalized absorbance - distance profiles of the selected lidocaine crystals are shown in Fig. 7D. Based on this procedure, the resolution of the SDI imaging system at 254 nm with the pixels binned 4 × 4 was estimated to be 250 and 75 µm in the x- and y-directions, respectively. Table 2 shows the estimated resolution from the crystals by the SDI system with pixels binned 1 × 1 and 4 × 4 at 254 and 610 nm. Overall, these data indicate that pixel binning is not the limiting factor when it comes to resolution; the dimension of the light emitting slit and shadowing effects seem to be significant contributing factors.

3.2 Effects of hydrogels on density effects

The dissolution behavior of lidocaine from selected single crystals into stagnant phosphate buffer has previously been investigated by UV imaging. The study showed that the dissolved lidocaine seems to gather at the bottom of the quartz cell, which may be explained by the formation of a density gradient as lidocaine dissolves leading to natural convection [16]. Hydrogel matrixes have been shown to suppress natural convection due to density gradients [43,48-50]. In the current study, the effect of introducing a 0.5% (w/v) agarose hydrogel at pH 7.4 as a dissolution medium on the dissolution behavior of a single lidocaine crystal under stagnant conditions was visualized. Fig. 8 shows the absorbance maps of the dissolution behavior of lidocaine. The image resolution is not affected by introduction of the gel (Fig. 8), which is understandable in the light of the discussion in section 3.1, and the crystals are still readily apparent. During dissolution of lidocaine in the hydrogel matrix, the absorbance contours mapped around the crystals were almost symmetrical (Fig. 8A). This contrasts with the irregular contours around the crystals in the phosphate buffered solution (Fig. 8B). The symmetrical absorbance maps formed in the hydrogel matrix indicate that the natural convection seen in aqueous solution has been effectively suppressed in the hydrogel matrix. The mass transport of dissolved lidocaine in the hydrogel is solely due to diffusion whereas transport of dissolved lidocaine the solution is due to convective currents as well as diffusion.

3.3 Lidocaine diffusion in hydrogel

Diffusion coefficients of drug compounds in hydrogel matrixes have previously been determined by fitting data to equations based on Fick's second law [21,42]. In these studies, the samples are placed in a manner such that the diffusion can be assumed to occur only in the x-direction. The determined diffusion coefficients are influenced by the defined position of the interface, x_0 (cf. Eq. 1), and the precision with which the position of the interface can be determined may therefore be important for the results obtained. In our previous diffusion studies using a D100 imaging system [21,42], the interface between the sample and the release (acceptor) medium was perpendicular to the fibre optic line source, i.e. oriented such that diffusion occur in x-direction where the imaging system has the lowest resolution. The results in section 3.1.2 showed that the orientation of the objects relative to the line light source has a significant impact on the resolution. Tests were therefore undertaken to check whether rotation of the output end of the round-to-line fibre optic cable by 90° influenced the initial appearance and sharpness of the interface between a hydrogel loaded with lidocaine and a blank hydrogel. Interestingly, no difference in the sharpness of the boundary between the hydrogels was observed (data not shown), and the slopes of the tangent to the curves at the interface were similar at time zero. However, the curves were associated with more scatter when the line source was rotated 90°, which may be attributed to the higher resolution in this direction. By applying Eq. 1 to the normalized absorbance-distance profiles (Fig. 9A), diffusion coefficients of lidocaine in the hydrogel matrixes were determined. The apparent diffusion coefficients were found to decrease with time (10 - 180 min). By plotting the diffusion coefficient as a function of the reciprocal of time (Fig. 9B), the apparent diffusion coefficient was obtained from the intercept of the straight line with the y-axis [21,51]. The diffusion coefficient was determined to be $(6.3 \pm 0.05) \times 10^{-10}$ m^2/s, $(6.9 \pm 0.05) \times 10^{-10}$ m^2/s and $(7.5 \pm 0.11) \times 10^{-10}$ m^2/s ($n = 3 \times 3$) at 22.0 ± 1.0 °C using

404 the D100, SDI and D100 system with the line rotated 90°, respectively. Brouneus and co-
405 workers have determined the diffusion coefficient of lidocaine hydrochloride to be (7.49 ± 0.43)
406 × 10^{-10} m^2/s (n = 8) in 1% (w/w) agarose gel at 25 °C by measuring the amount of lidocaine
407 diffusing from a well stirred solution of 25 mM lidocaine into the gel at specified time points
408 [52]. The diffusion coefficient of lidocaine in phosphate buffered solution was determined to be
409 (5.8 ± 0.2) × 10^{-10} m^2/s using TDA, which is in accordance with the previously determined
410 diffusion coefficient of lidocaine in buffer solution at pH 7.4 ((5.5 ± 0.2) × 10^{-10} m^2/s) [32]. Due
411 to the unhindered diffusion of small molecules in the agarose hydrogel matrix, the diffusion
412 coefficient of lidocaine obtained in the hydrogel was expected to be comparable to the value
413 obtained in aqueous solution. The observed variation in the obtained diffusion coefficients for
414 lidocaine in agarose gels and in solution is within the normal range, when different methods are
415 applied. Using the current UV imaging instrumentation, where the effective height in the y-
416 direction is 3.9 mm and the length in the x-direction is ~ 8 mm for the setup used for the
417 diffusion experiments, it is advantageous to study diffusion in the x-direction due to a longer
418 potential diffusion distance allowing the process to be followed for longer periods of time. The
419 effective imaging area in the x-direction is 7 - 9 mm in the D100 and SDI system, while it is 4 - 6
420 mm in the D100 system with the line of fibres rotated 90° and the fall of intensity with distance
421 as noted in Fig. 2A. The reason why a difference with respect to sharpness of the interface was
422 not observed using the different UV imaging setups may be due to the immediate diffusion of
423 lidocaine as the lidocaine loaded gel is placed side by side with the blank hydrogel matrix. The
424 time for the quartz cell containing the sample to be placed under the UV imaging sensor head
425 varies between experiments and is generally in the order of 1 to 5 min. The root-mean-square
426 distances ($<x^2>^{½}$) of lidocaine at 1 and 5 min were calculated to be 300 and 670 µm,

respectively, using the formula for one-dimensional diffusion $\langle x^2 \rangle^{½} = \sqrt{(2 \times D \times t)}$ and a diffusion coefficient of 7.5×10^{-10} m^2/s. These are relatively large distances, in comparison to the resolution which is in the order of 20 to 200 µm. Thus, the experimental procedure rather than instrument performance appears to be the limiting factor in these diffusion assays.

4. Conclusion

The present study showed that the apparent absorption coefficients depend on the spectroscopic instrumentation used, highlighting the importance of investigating the linearity prior to dissolution imaging. For quantitative results, the apparent molar absorption coefficient should be determined using the UV imaging system rather than a conventional spectrophotometer.

The main difference between the D100 and SDI imaging systems is the introduction of a collimating lens in the latter system. This leads to several improvements in instrument performance. The SDI imaging system showed an increased uniformity of the light intensity across the imaging area as well as an improved resolution, which may be explained by a reduced shadowing effect. Both systems have as light source a line of 100 µm fibres aligned in the x-direction, which means that resolution is greatest in the y-direction. The main parameter influencing the resolution was found to be the distance of the object above the cover slip and the sensor surface, consistent with the optical lever effect. Under the most favorable conditions, with a grid placed directly on the cover slip, the resolution was estimated to 12.5 and 16.7 lp/mm in the x- and y-directions, respectively. Effects related to positioning of objects should therefore be taken into account during designing of experiments and image interpretation.

UV imaging offers detailed insights into dissolution processes as shown for lidocaine crystals. In aqueous solution, natural convection leads to dense lidocaine solution accumulating at the bottom of the cell. Agarose gels are shown to be able to suppress the effect of natural convection arising from density gradients, in accordance with previous studies [16]. Hydrogels may thus be suitable matrixes for visualizing and characterizing dissolution (and release) processes under stagnant conditions. In relation to studying diffusion processes in hydrogels, the positioning of the diffusion boundary relative to the fibre optic line source (parallel versus perpendicular) did not improve the sharpness of the interface even at the shortest measurement time. Calculations of root-mean-square distances for diffusion showed that this could have been due to diffusion occurring as the experiment was being setup, rather than the instrument limiting the sharpness of the diffusion boundary.

The knowledge obtained in the current study about the instrument performance characteristics will be helpful in the design and interpretation of UV imaging based release and dissolution studies.

Acknowledgements

This project has received funding from the European Union's Horizon 2020 research and innovation program under the Marie Sklodowska-Curie grant agreement No 644056. The authors alone are responsible for the content and writing of this paper.

References

[1] J. Emami, In vitro - in vivo correlation: from theory to applications, J. Pharm. Pharmc. Sci. 9 (2006) 169-189.

[2] M. Windbergs, D.A. Weitz, Drug dissolution chip (DDC): A microfuidic approach for drug release. Small 7 (2011) 3011-3015.

[3] M. Kuentz, Analytical technologies for real-time drug dissolution and precipitation testing on a small scale, J. Pharm. Pharmacol. 67 (2014) 143-159.

[4] A.V. Ewing, G.S. Clarke, S.G. Kazarian, Attenuated total reflection-Fourier transformed infrared spectroscopic imaging of pharmaceuticals in microfluidic devices, Biomicrofluidics 10 (2016) 024125.

[5] K. Mäder, G. Bacic, A. Domb, O. Elmalak, R. Langer, H.M. Swartz, Noninvasive in vivo monitoring of drug release and polymer erosion from biodegradable polymers by EPR spectroscopy and NMR imaging, J. Pharm. Sci. 86 (1997) 126-134.

[6] J.C. Richardson, R.W. Bowtell, K. Mäder, C.D. Melia, Pharmaceutical applications of magnetic resonance imaging (MRI), Adv. Drug Deliv. Rev. 57 (2005) 1191-1209.

[7] K.P. Nott, Magnetic resonance imaging of tablet dissolution, Eur. J. Pharm. Biopharm. 74 (2010) 78-83.

[8] C. Chen, L.F. Gladden, M.D. Mantle, Direct visualization of in vitro drug mobilization from lescol XL tablets using two-dimensional ^{19}F and ^{1}H magnetic resonance imaging, Mol. Pharm. 11 (2013) 630-637.

[9] S.G. Kazarian, J. van der Weerd, Simultaneous FTIR spectroscopic imaging and visible photography to monitor tablet dissolution and drug release, Pharm. Res. 25 (2008) 853-860.

[10] J.A. Kimber, S.G. Kazarian, F. Stepanek, Microstructure-based mathematical modelling and spectroscopic imaging of tablet dissolution, Comput. Chem. Eng. 35 (2011) 1328-1339.

[11] S.G. Kazarian, A.V. Ewing, Applications of Fourier transform infrared spectroscopic imaging to tablet dissolution and drug release, Expert Opin. Drug Deliv. 10 (2013) 1207-1221.

[12] M. Windbergs, M. Jurna, H.L. Offerhaus, J.L. Herek, P. Kleinebudde, C.J. Strachan, Chemical imaging of oral solid dosage forms and changes upon dissolution using coherent anti-stokes Raman scattering microscopy, Anal. Chem. 81 (2009) 2085-2091.

[13] G.S. Bajwa, K. Hoebler, C. Sammon, P. Timmins, C.D. Melia, Microstructural imaging of early gel layer formation in HPMC matrices, J. Pharm. Sci. 95 (2006) 2145-2157.

[14] F. Brandl, F. Kastner, R.M. Gschwind, T. Blunk, J. Tessmar, A. Göpferich, Hydrogel-based drug delivery systems: Comparison og drug diffusivity and release kinetics, J. Control. Release 142 (2010) 221-228.

[15] J.P. Boetker, M. Savolainen, V. Koradia, F. Tian, T. Rades, A. Müllertz, C. Cornett, J. Rantanen, J. Østergaard, Insights into the early dissolution events of amlodipine using UV imaging and Raman spectroscopy, Mol. Pharm. 8 (2011) 1372-1380.

[16] J. Østergaard, F. Ye, J. Rantanen, A. Yaghmur, S.W. Larsen, C. Larsen, H. Jensen, Monitoring lidocaine single-crystal dissolution by ultraviolet imaging, J. Pharm. Sci. 100 (2011) 3405-3410.

[17] W.L. Hulse, J. Gray, R.T. Forbes, A discriminatory intrinsic dissolution study using UV area imaging analysis to gain additional insights into the dissolution behaviour of active pharmaceutical ingredients, Int. J. Pharm. 434 (2012) 133-139.

[18] M. Li, N. Qiao, K. Wang, Influence of sodium lauryl sulfate and tween 80 on carbamazepine-nicotinamide cocrystal solubility and dissolution behaviour, Pharmaceutics 5 (2013) 508-524.

[19] N. Qiao, K. Wang, W. Schlindwein, A. Davies, M. Li, In situ monitoring of carbamazepine-nicotinamide cocrystal intrinsic dissolution behaviour, Eur. J. Pharm. Biopharm. 83 (2013) 415-426.

[20] J. Østergaard, J. Lenke, S.S. Jensen, Y. Sun, Y. Fengbin, UV imaging for in vitro dissolution and release studies: Initial experiences, Dissolut. Technol. 22 (2014) 27-38.

[21] F. Ye, A. Yaghmur, H. Jensen, S.W. Larsen, C. Larsen, J. Østergaard, Real-time UV imaging of drug diffusion and release from Pluronic F127 hydrogels, Eur. J. Pharm. Sci. 43 (2011) 236-243.

[22] J. Østergaard, E. Meng-Lund, S.W. Larsen, C. Larsen, K. Petersson, J. Lenke, H. Jensen, Real-time UV imaging of nicotine release from transdermal patch, Pharm. Res. 27 (2010) 2614-2623.

[23] J. Østergaard, J.X. Wu, K. Naelapaa, J.P. Boetker, H. Jensen, J. Rantanen, Simultaneous UV imaging and raman spectroscopy for the measurement of solvent-mediated phase transformations during dissolution testing, J. Pharm. Sci. 103 (2014) 1149-1156.

[24] F. Ye, S.W. Larsen, A. Yaghmur, H. Jensen, C. Larsen, J. Østergaard, Drug release into hydrogel-based subcutaneous surrogates studied by UV imaging, J. Pharm. Biomed. Anal. 71 (2012) 27-34.

[25] Y. Lu, L. Mingzhong, Simultaneous rapid determination of the solubility and diffusion coefficients of poorly water-soluble drug based on a novel UV imaging system, J. Pharm. Sci. 105 (2016) 131-138.

[26] N. Gautschi, P.V. Hoogevest, M. Kuentz, Amorphous drug dispersions with mono- and diacyl lecithin: On molecular categorization of their feasibility and UV dissolution imaging, Int. J. Pharm. 491 (2015) 218-230.

[27] S.S. Jensen, H. Jensen, E.H. Møller, C. Cornett, F. Siepmann, J. Siepmann, In vitro release studies of insulin from lipid implants in solution and in a hydrogel matrix mimicking the subcutis, Eur. J. Pharm. Sci. 81 (2016) 103-112.

[28] F. Oukacine, L. Garrelly, B. Romestand, D.M. Goodall, T. Zou, H. Cottet, Focusing and mobilization of bacteria in capillary electrophoresis, Anal. Chem. 83 (2011) 1571-1578.

[29] P.L. Urban, D.M. Goodall, E.T. Bergström, N.C. Bruce, Electrophoretically mediated microanalysis of a nicotinamide adenine dinucleotide-dependent enzyme and its facile multiplexing using an active pixel sensor UV detector, J. Chromatogr. A 1162 (2007) 132-140.

[30] ISO 12233:2014(en) Photography - Electronic still picture imaging - Resolution and spatial frequency responses. International Organization for Standardization, Geneva, Switzerland. https://www.iso.org/obp/ui/#iso:std:iso:12233:ed-2:v1:en. 2015 (Accessed 25-06-2015).

[31] J. Crank The mathematics of diffusion, Oxford University Press, Oxford, 1975.

[32] F. Ye, H. Jensen, S.W. Larsen, A. Yaghmur, C. Larsen, J. Østergaard, Measurement of drug diffusivities in pharmaceutical solvents using Taylor dispersion analysis, J. Pharm. Biomed. Anal. 61 (~~2011~~2012) 176-183.

[33] M. Kulp, P.L. Urban, M. Kaljurand, E.T. Bergström, D.M. Goodall, Visualization of electrophoretically mediated in-capillary reactions using a complementary metal oxide semiconductor-based absorbance detector, Anal. Chim. Acta 570 (2006) 1-7.

[34] P.L. Urban, D.M. Goodall, E.T. Bergstrom, N.C. Bruce, Electrophoretic assay for penicillinase: Substrate specificity screening by parallel CE with an active pixel sensor, Electrophoresis 28 (2007) 1926-1936.

[35] P.L. Urban, D.M. Goodall, A.Z. Carvalho, E.T. Bergström, A. Van Schepdael, N.C. Bruce, Multi-compound electrophoretic assays for tyramine oxidase with a UV area detector imaging multiple windows on a looped capillary, J. Chromatogr. A 1206 (2008) 52-63.

[36] J. Østergaard, H. Jensen, Simultaneous evaluation of ligand binding properties and protein size by electrophoresis and Taylor dispersion in capillaries, Anal. Chem. 81 (2009) 8644-8648.

[37] S. Chatterjee, V. Shanker, P.K. Ghosh, Trapping parameters and kinetics in Gd_2O_2S:Tb phosphor, Solid state Commun. 80 (1991) 877-880.

[38] M.M. Blouke, M.W. Cowens, J.E. Hall, J.A. Westphal, A.B. Christensen, Ultraviolet downconverting phosphor for use with silicon CCD imagers, Appl. Opt. 19 (1980) 3318-3321.

572 [39] M.W. Cowens, M.M. Blouke, T. Fairchild, J.A. Westphal, Coronene and liumogen as VUV
573 sensitive coatings for Si CCD imagers: a comparison, Appl. Opt. 19 (1980) 3727-3728.

574 [40] J.P. Boetker, J. Rantanen, T. Rades, A. Müllertz, J. Østergaard, H. Jensen, A new approach
575 to dissolution testing by UV imaging and finite element simulations, Pharm. Res. 30 (2013)
576 1328-1337.

577 [41] J. Østergaard, E. Meng-Lund, S. Larsen, C. Larsen, K. Petersson, J. Lenke, H. Jensen, Real-
578 Time UV imaging of nicotine release from transdermal patch, Pharm. Res. 27 (2010) 2614-
579 2623.

580 [42] S.S. Jensen, H. Jensen, C. Cornett, E.H. Møller, J. Østergaard, Insulin diffusion and self-
581 association characterized by real-time UV imaging and Taylor dispersion analysis, J. Pharm.
582 Biomed. Anal. 92 (2014) 203-210.

583 [43] M.H. Gaunø, T. Vilhelmsen, C.C. Larsen, J.P. Boetker, J. Wittendorff, J. Rantanen, J.
584 Østergaard, Real-time in vitro dissolution of 5-aminosalicylic acid from single ethyl
585 cellulose coated extrudates studied by UV imaging, J. Pharm. Biomed. Anal. 83 (2013) 49-
586 56.

587 [44] S. Görög *Ultraviolet-visible spectrophotometry in pharmaceutical analysis*, CRC Press,
588 Boca Raton, 1995.

589 [45] L. Sommer *Analytical absorption spectrophotometry in the visible and ultraviolet: The*
590 *principles*, Elsevier Science Publishers, Amsterdam, 1989.

591 [46] D.S. Hage, J.D. Carr *Analytical chemistry and quantitative analysis*, Prentice Hall, Boston,
592 2011.

593 [47] K.L. Chan, S.G. Kazarian, New opportunities in micro- and macro-attenuated total reflection
594 infrared spectroscopic imaging: spatial resolution and sampling versatility, Appl. Spectrosc.
595 57 (2003) 381-389.

596 [48] S.S. Jensen, H. Jensen, C. Cornett, E.H. Møller, J. Østergaard, Real-time UV imaging
597 identifies the role of pH in insulin dissolution behavior in hydrogel-based subcutaneous
598 tissue surrogate, Eur. J. Pharm. Sci. 69 (2015) 26-36.

599 [49] B. Lorber, C. Sauter, A. Theobald-Dietrich, A. Moreno, P. Schellenberger, M.C. Robert, B.
600 Capelle, S. Sanglier, N. Potier, R. Giege, Crystal growth of proteins, nucleic acids, and
601 viruses in gels, Prog. Biophys. Mol. Biol. 101 (2009) 13-25.

602 [50] J.M. Garcia-Ruiz, M.L. Novella, R. Moreno, J.A. Gavira, Agarose as crystallization media
603 for proteins I: transport processes, J. Cryst. Growth 232 (2001) 165-172.

604 [51] V.F. Felicetta, A.E. Markham, Q.P. Peniston, J.L. McCarthy, A study of diffusion in agar
605 gels by a light absorption method, J. Am. Chem. Soc. 71 (1949) 2879-2885.

606 [52] F. Brouneus, K. Karami, P. Beronius, L.O. Sundelöf, Diffusive transport properties of some
607 local anesthetics applicable for iontophoretic formulation of the drugs, Int. J. Pharm. 218
608 (2001) 57-62.

609 **Figures:**

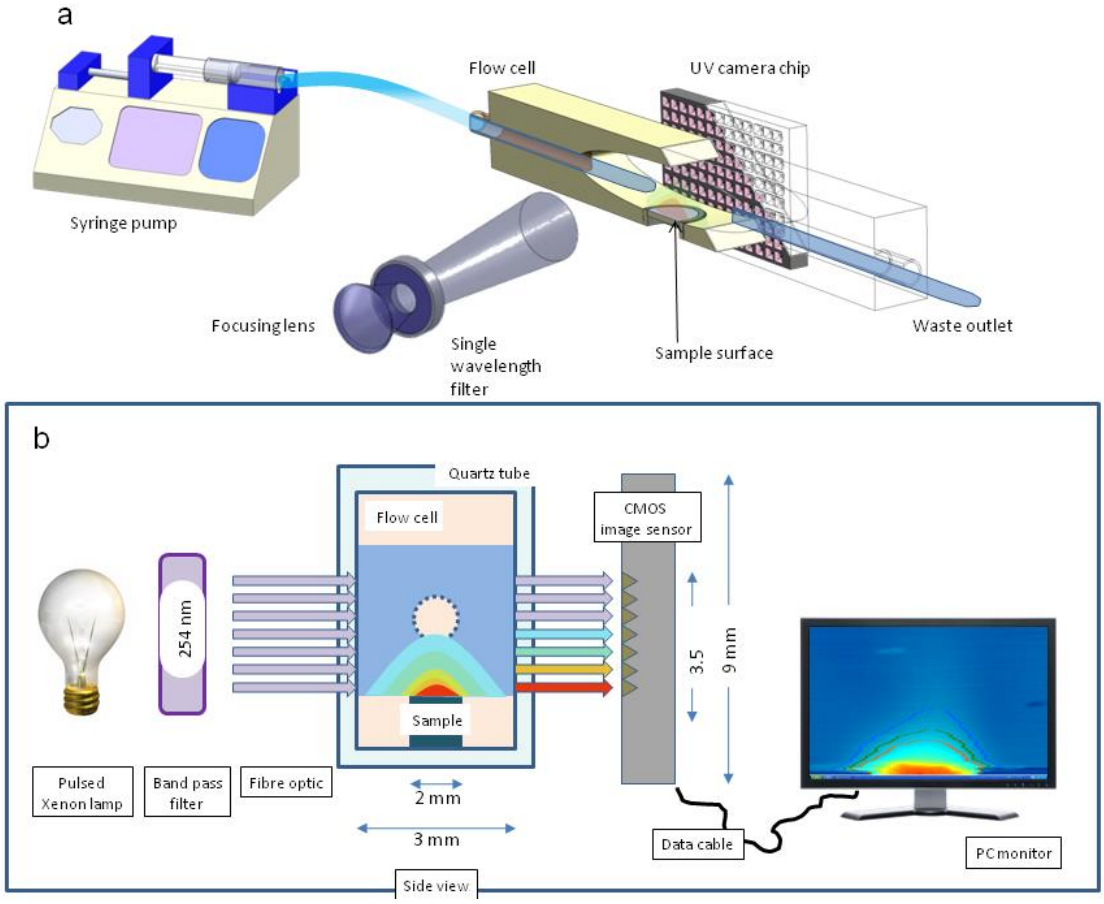

610

611 **Fig. 1.** Schematic representation of the UV imaging setup (reprinted from [22] with permission

612 from Springer).

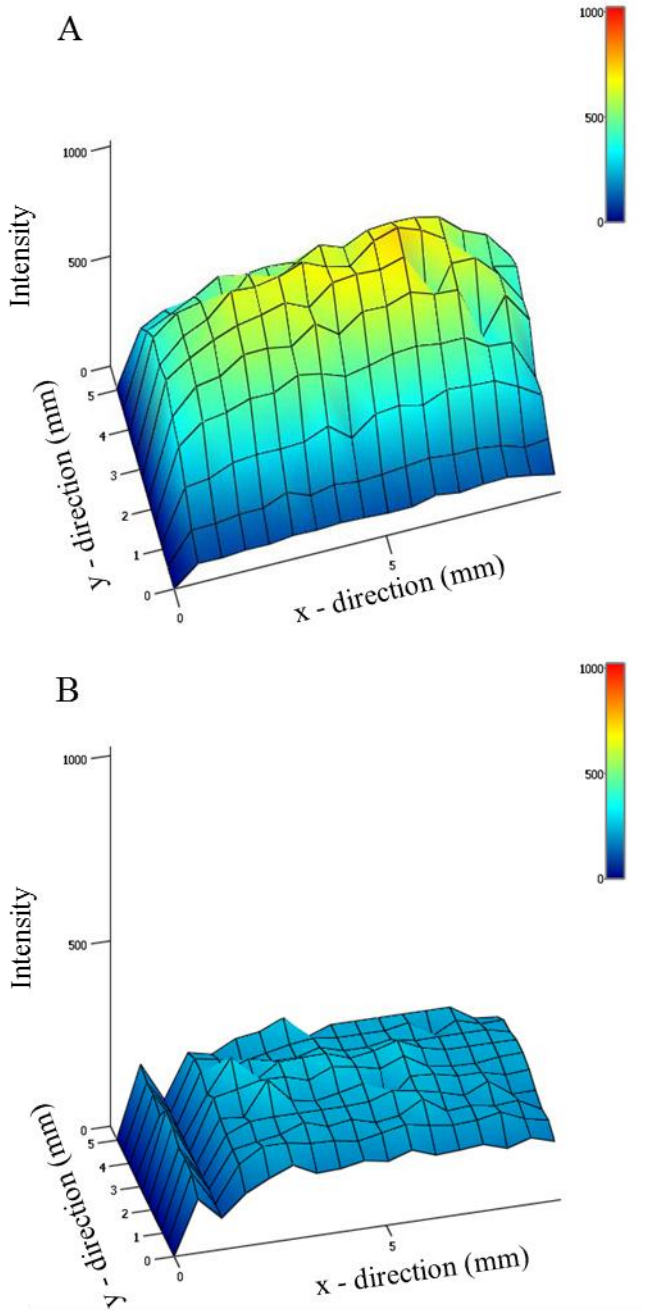

613

614 **Fig. 2.** Light intensity maps of the imaging area in the x- and y-direction of the A) ActiPix D100

615 UV area imaging system (Paraytec Ltd, York, UK) and B) Sirius SDI (Sirius Analytical Ltd, East

616 Sussex, UK) imaging system with pixels binned 1 × 1 at 254 nm.

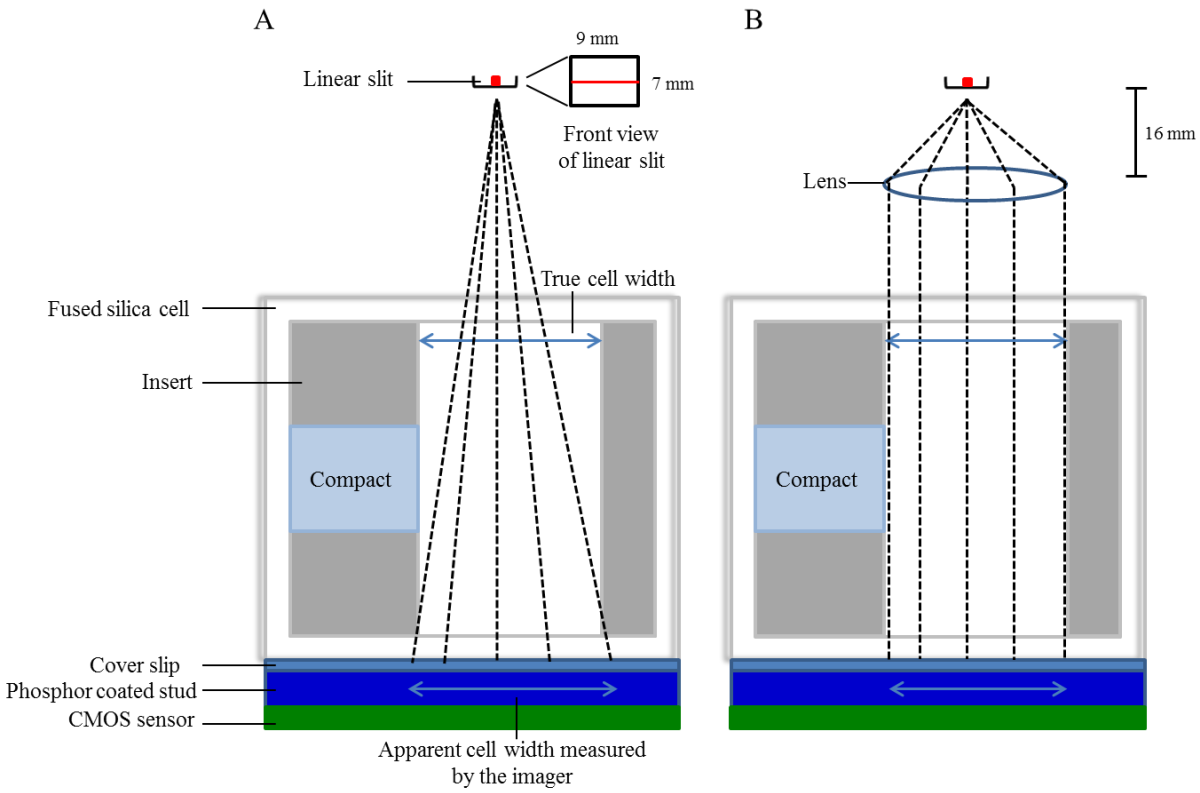

617

618 **Fig. 3.** Schematic illustration of sensor head components and light paths for the D100 (A) and

619 SDI (B) imaging systems. The drawings are not to scale, and the linear slit height is 16 mm

620 above the cylinder lens. Note the change in sensor head orientation relative to Fig. 1.

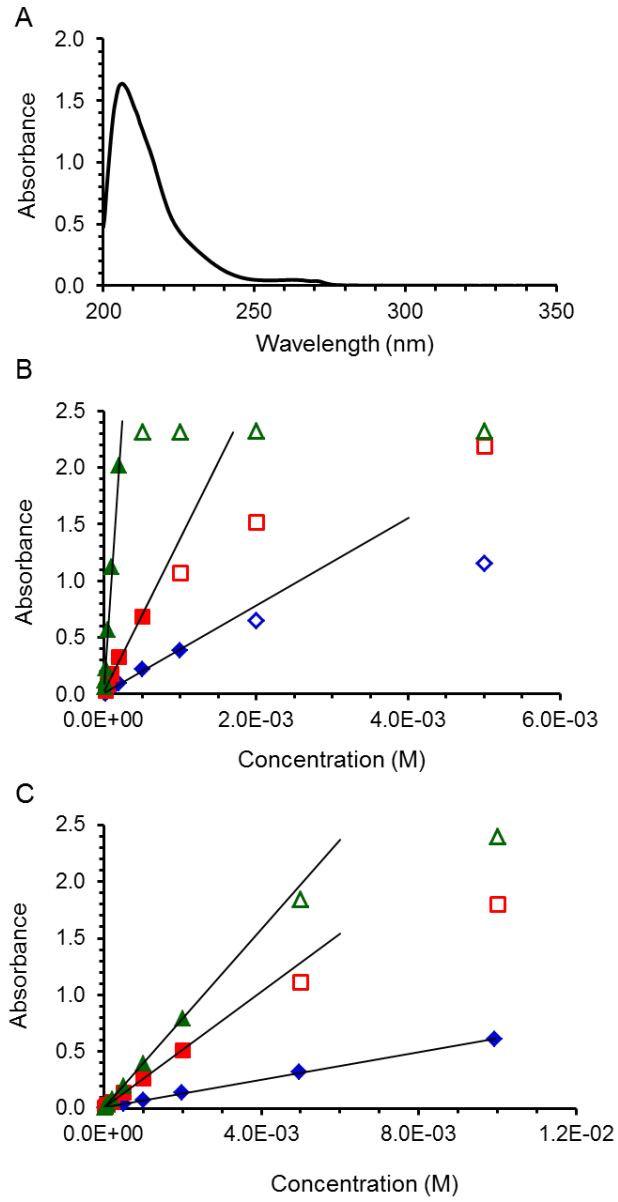

621

622 **Fig. 4.** A) UV scan of 1.0×10^{-4} M lidocaine in 0.067 M phosphate buffered solution, pH 7.4,
623 obtained using a conventional spectrophotometer. Calibration curves of lidocaine in phosphate
624 buffered solution at pH 7.4 obtained in quartz cells with a light path of 1 (♦, ◇) and 4 mm (■, □)
625 using the SDI UV imaging and 10 mm (▲, Δ) by a conventional spectrophotometer at B) 214
626 and C) 254 nm. The lines are the linear regression using only the closed symbols, and the open
627 symbols represent the points that are deviating from linearity.

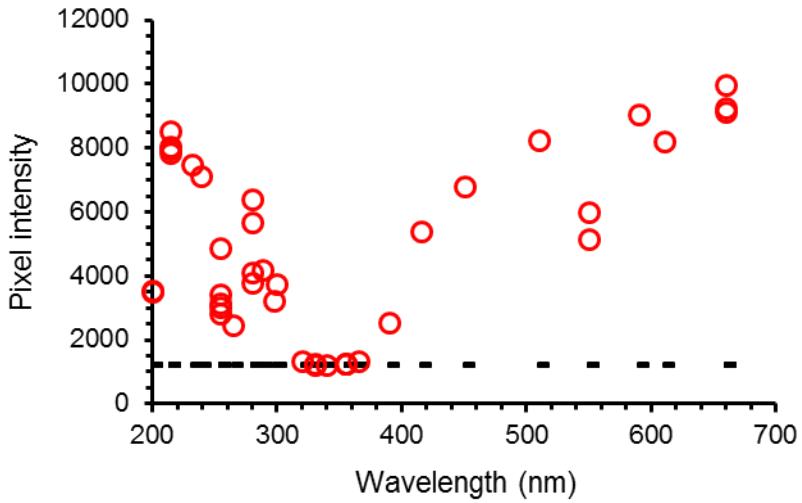

Fig. 5. Pixel intensities as a function of wavelength for the interference band-pass filters using the SDI UV imaging instrument (○), and the measured intensities (the dark current), when the lamp was turned off (▬). The pixel intensities plotted were average values read from a selected image area (5.60 × 4.76 mm^2). At some wavelengths, the pixel intensity was measured by several filters, some of which had different transmission efficiency. All filters were measured on the same system in a single experimental session.

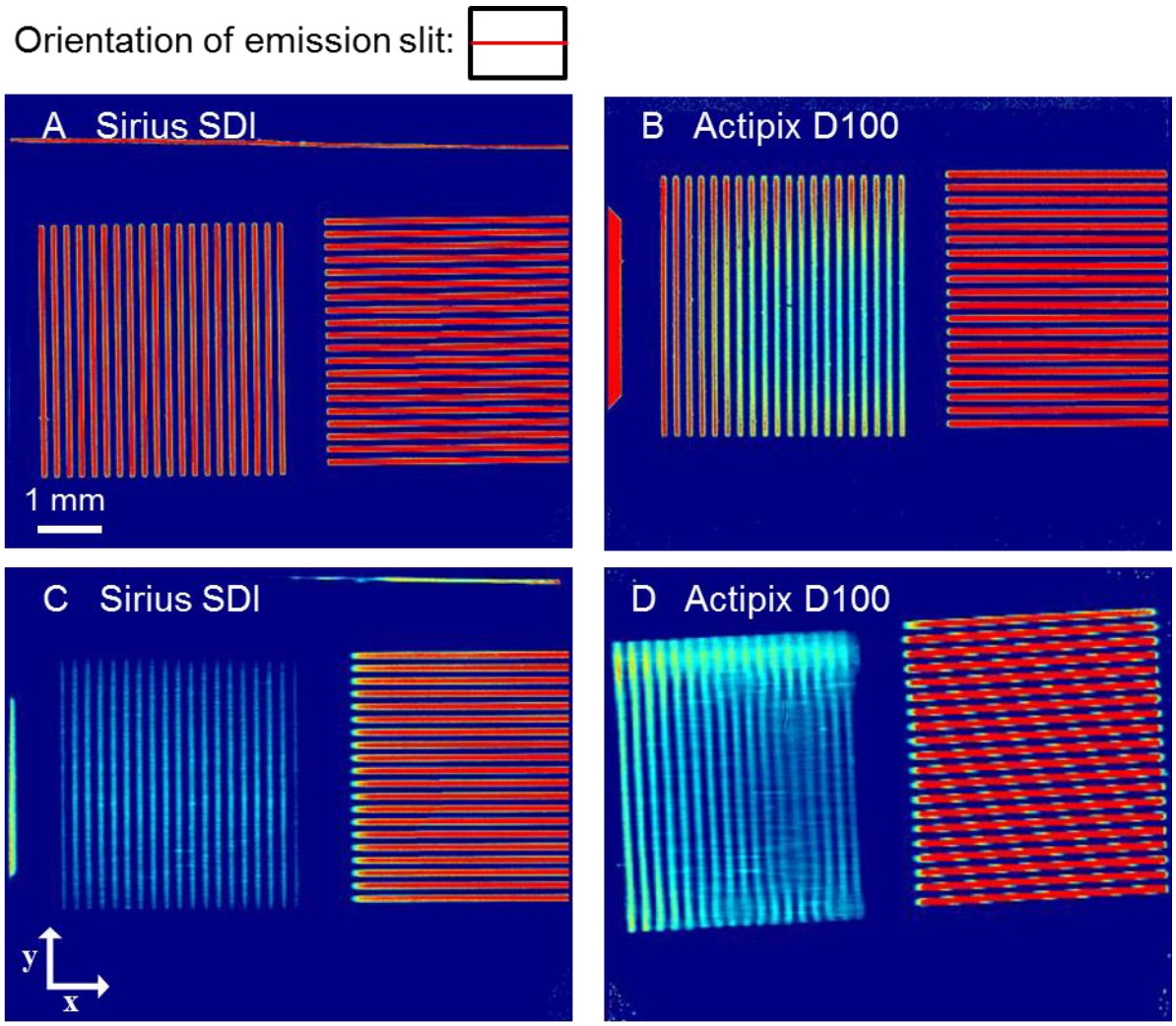

Fig. 6. Absorbance maps of the grids obtained by the ActiPix D100 UV Area Imaging (Paraytec Ltd, York, UK) and Sirius SDI (Sirius Analytical Ltd, East Sussex, UK) imaging system with pixels binned 1 × 1 at 610 nm, when the bar pattern grids (100 µm line width, 100 µm vacancy before repeat) were placed on the cover slip of the sensor surface (A and B) and on quartz cells, placing the grid 1.2 mm above the cover slip of the sensor surface (C and D). Images are 9.0 × 7.2 mm^2 and the absorbance values range between 0 mAU (dark blue) and ~1400 mAU (red).

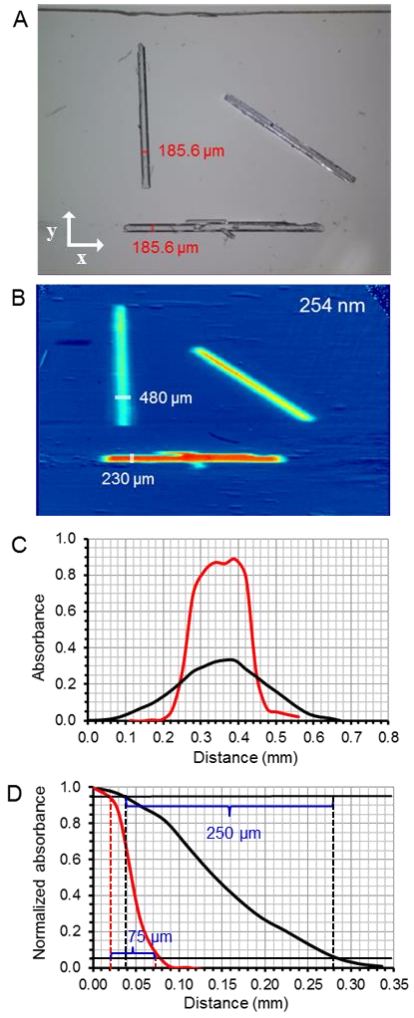

642

643 **Fig. 7.** A) Microscope photograph (the image is 8.3 × 6.4 mm^2) and B) absorbance maps of the
644 lidocaine crystals arranged in a quartz cell obtained by the Sirius SDI imaging system with pixels
645 binned 4 × 4 at 254 nm. The image is 10.4 × 4.6 mm^2. C) Absorbance – y-distance profile of the
646 lidocaine crystal placed in the x-direction (—) and absorbance – x-distance profile for crystal
647 placed in the y-direction (—) for determining the width of the crystals from the absorbance maps
648 and D) normalized absorbance - distance profile of one side of a lidocaine crystal placed in the x-
649 direction (—) and y-direction (—) for estimating the resolution of the Sirius SDI imaging
650 system.

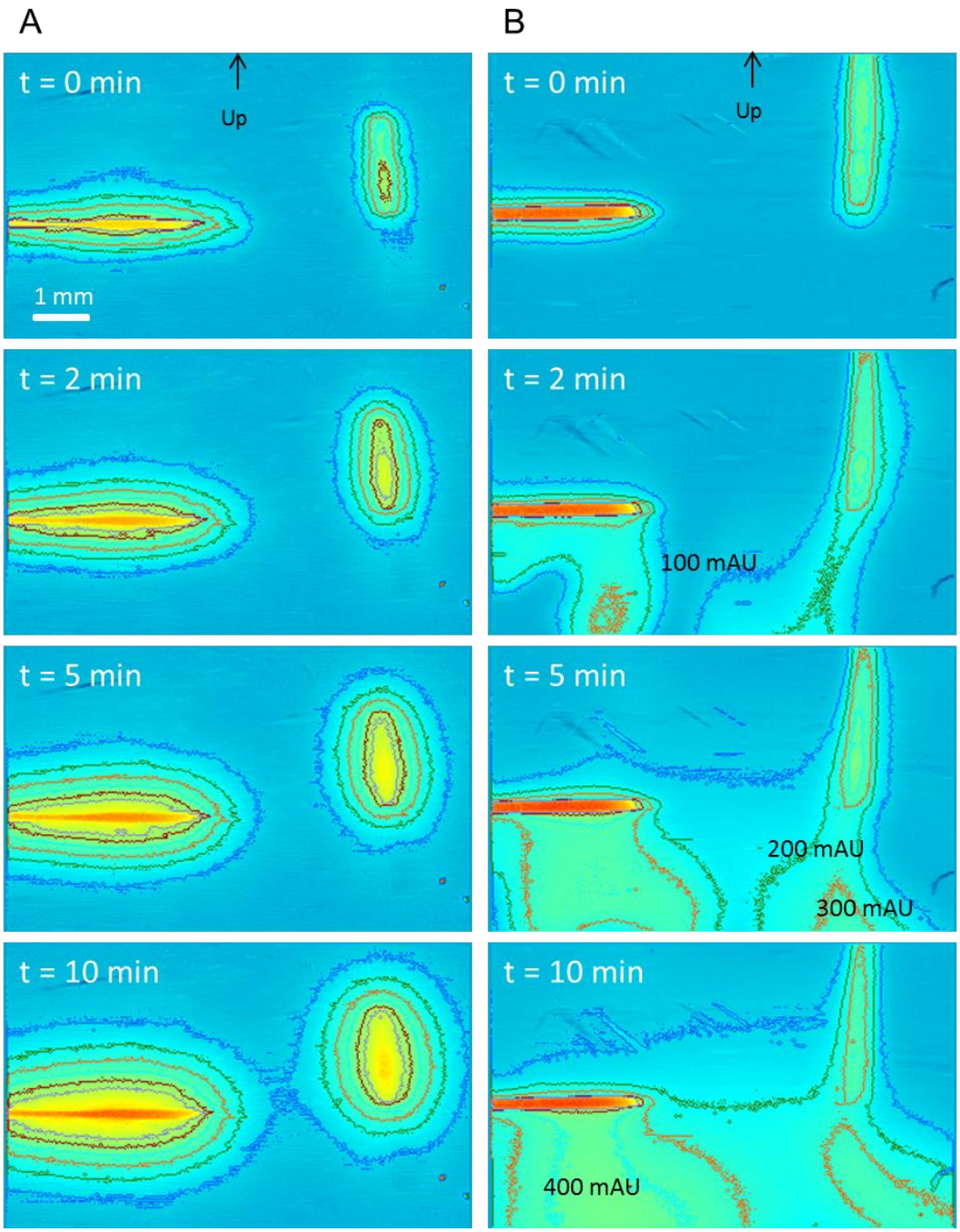

Fig. 8. Time-dependent absorbance contour maps of the dissolution of lidocaine crystals in A) 0.5% (w/v) agarose gel, pH 7.4 and B) 0.067 M phosphate buffered solution, pH 7.4. The dissolution was performed in quartz cells with 1 mm light path using the Sirius SDI UV imaging system with the pixels binned 4 × 4 at 254 nm and the sensor head placed in the upright position.

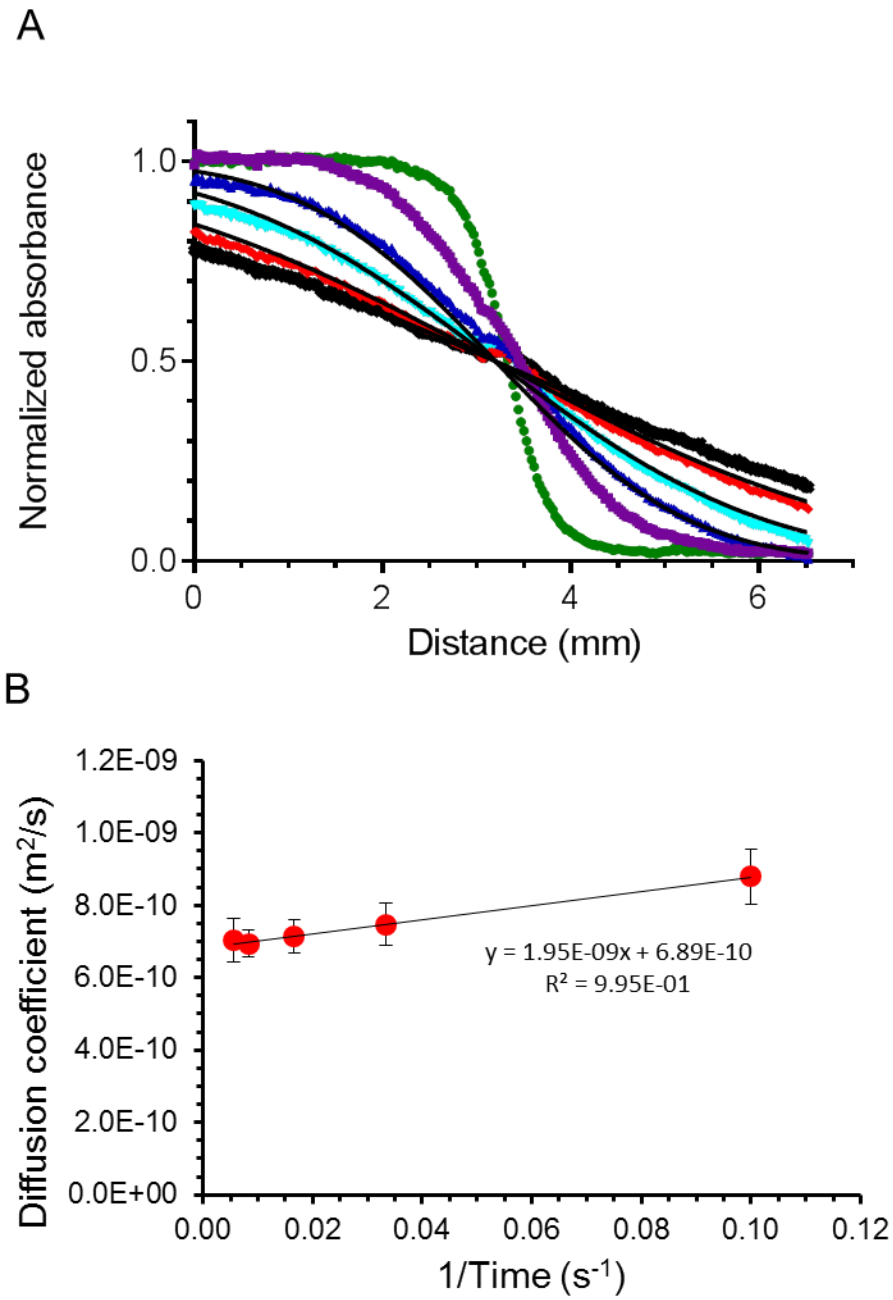

656

657 **Fig. 9.** A) Absorbance – distance profiles for lidocaine diffusion in 0.5% (w/v) agarose hydrogel

658 matrix, pH 7.4, after 0 (●), 10 (■), 30 (▲), 60 (▼), 120 (♦) and 180 min (+) obtained using the

659 Sirius SDI system. The black lines represent the fits to Eq. (1). B) Fitted diffusion coefficients of

660 lidocaine in 0.5% (w/v) agarose hydrogel matrix, pH 7.4, as a function of the inverse of time.